Non-invasive Material Characterization using SystemID with Temperature Modulated Raman Spectroscopy

Alex Urpi, Álvaro Fernández-Galiana, Hilary Johnson, S.N.R. Kantareddy, Zeguan Wang

***Abstract*—Non-invasive material characterization techniques have wide applications in a variety of fields including healthcare. One of the most researched problems in this area is identifying blood glucose concentrations without drawing a blood sample. In this paper, we build a temperature-modulated confocal Raman spectrometer to identify material samples. We tested our system on diamond samples with artificial noise to simulate glucose underneath the skin. Our results show that by using temperature modulated laser wavelength, noise can be removed, improving the signal to noise from 2.9 to 4.3. We also show how we performed a system identification analysis of our laser setup to obtain a transfer function for fast material scanning applications.**

***Index Terms*—System-ID, Raman Spectroscopy, Non-invasive material characterization, Glucose monitoring**

I. Introduction

WEARABLES enable us to continuously monitor different human body parameters such as heart rate, sleep cycle, physical activity etc., transforming our approach towards health from reactionary care to preventive care [1]. Wearables of the future will also enable us to monitor critical chemical parameters such as blood glucose levels leading to non-invasive lab-on-the-body diagnostics. However, analyzing sub-dermal molecular concentrations is more challenging than measuring external physical parameters. The objective of our work is to non-invasively identify blood glucose concentrations through optical methods.

In this work, we explored Raman spectroscopy techniques for material identification. Four phenomena occur when photons are incident on a material surface: transmission through the sample, fluorescence scattering, elastic scattering, and inelastic scattering. In inelastic scattering, reflected photons are lower or higher energy than the source due to the vibrations of the scattering molecule. Therefore, the energy of the photons is not conserved. Photons either lose energy, called Stokes scattering, or gain energy, called anti-Stokes scattering. This phenomenon is commonly known as Raman scattering and the result is scattered light with shifted frequency. We are interested in capturing these Raman scattered photons. These frequency shifts are characteristic to the chemical structure of the material. Therefore, Raman spectroscopy is a powerful tool for chemical analysis. However, Raman signals are weak, on the order of 1 in 10 million photons, and usually demonstrate peaks with intense fluorescence background. Therefore, a challenge in using Raman spectroscopy is often separating the fluorescence background from the Raman signals. Our strategy to reduce this fluorescence background is to shift the excitation wavelength of the laser by modulating the temperature of the laser crystal. Raman spectra will shift in energy by the amount of shift in the excitation photons. However, any small changes in the excitation wavelength will not have significant effect on the fluorescence background. Therefore, by data processing on the spectra collected at different wavelengths, signal-to-noise ratio in identifying weak Raman signals can be enhanced. Noise reduction by shifting excitation frequency is a known property and the following subsection presents some evidence from the available literature.

Nithin, Alex, Hilary, Álvaro are with the Department of Mechanical Engineering, Massachusetts Institute of Technology, Cambridge, MA, 02139 USA e-mail:glucoid@mit.edu

Zeguan is with the Media Lab, Massachusetts Institute of Technology, Cambridge,

Manuscript received May, 2019

A. Prior art

Raman peak detection by taking the difference of two spectra obtained by slightly shifted excitation wavelengths is demonstrated on CHCl3 with added fluorescent laser dye [2]. In another study, confocal micro-Raman spectroscopy using shifted excitation difference techniques is also applied on single biological cells such as E.coli bacterial and red blood cells [3]. In another study, more than 2 excitation frequencies are used to improve the signal recovery by rejecting the fluorescence [4].

Our paper is organized as follows: Section II describes our method and experimental setup and Section III presents our results and future work.

II. Method and Experimental Setup

Raman scattering is a scarce phenomenon, in which only approximate one in 10^7 excitation photons can be converted into a Raman photon [5]. This extremely low yield poses a challenge to measure the Raman signals of a sample, especially when the detection noise level is high. Moreover, many materials also convert excitation light into fluorescence that are orders of magnitude stronger than the Raman signals. Thus, Raman signals become non-detectable in many cases primarily due to overwhelming fluorescence.

Raman scattering and fluorescent emissions are based on distinct mechanisms. In fluorescent emissions, photos are produced by state transitions from a high energy state to a

lower energy state of a molecule, while Raman scattering happens when an incident photo gains or loses the amount of energy of the first vibrational state by exciting the molecule to a transient intermediate energy state, or 'virtual state'. In other words, the wavelengths of fluorescent emissions is determined by the real energy states of a molecule and do not directly rely on the wavelength of incident photons. And the Raman photons, on the contrary, have a constant shift in wavenumbers regarding the wavelength of the excitation light. In addition, because the lifetime of a virtual state is much shorter than that of a real high energy state, Raman scattering processes usually complete in sub-nanoseconds, while fluorescent emissions can last for tens of nanoseconds [6].

Given the fundamentally difference of the physical principles of Raman scattering and fluorescent emissions, we can play several strategies to suppress the fluorescent noises of a Raman spectrum. One strategy is called time-gated detection, which takes advantages of the different lifetimes of the two processes. In this method, a super fast excitation light pulse (< 1 ns) is passed though a sample, and only the emission light within a short time window (sub-ns) from the excitation time point is detected. This time gating strategy efficiently collects the fast Raman photons while blocks the slow fluorescent emissions, greatly increasing the signal-to-noise ratios of a Raman spectrum. Ultrafast single photon detectors have been specifically designed for time-gated Raman spectroscopy, which can potentially contribute to the miniaturization of efficient Raman spectrometers [7][8].

In addition to special detectors, fast and powerful light sources, which can be cumbersome and costly, are also required for time-gated detection. Thus instead, we here decided to use another strategy, called shifted excitation Raman spectroscopy, to extract Raman spectrums from the fluorescent and environmental noises. This methods relies on the fact that Raman spectrums shift accordingly with the wavelength of incident light, while fluorescence and environmental noises do not. By tuning the wavelength of excitation light, we can obtain multiple superpositions of constant fluorescent and environmental noises and Raman spectrums that shift the same amount as the incident light in wavenumbers. Post signal processing enables us to extract only the shifted components in the data, which corresponds to the Raman spectrum.

A. Confocal Raman Microscope

In order to accurately measure the Raman spectrums with shifted excitation wavelengths, we built a confocal Raman microscope with a temperature control module which can shift the wavelength of the excitation laser (Fig. 1). Here, a 670 nm laser diode (CPS670F, 4.5 mW, Thorlabs) was installed in a customized temperature control module as the excitation light source. In order to remove the undesired optical modes of the laser, the output beam was directed through a spatial filter (C260TMD-B, Thorlabs; P25D, Thorlabs) using two mirrors, and then was expanded and collimated through a 50 mm focal-length lens (LBF254-050-B, Thorlabs) to a beam diameter of approximately 10 mm. The expanded beam then hit a 685 nm long pass dichroic mirror (FF685-Di02-25x36,

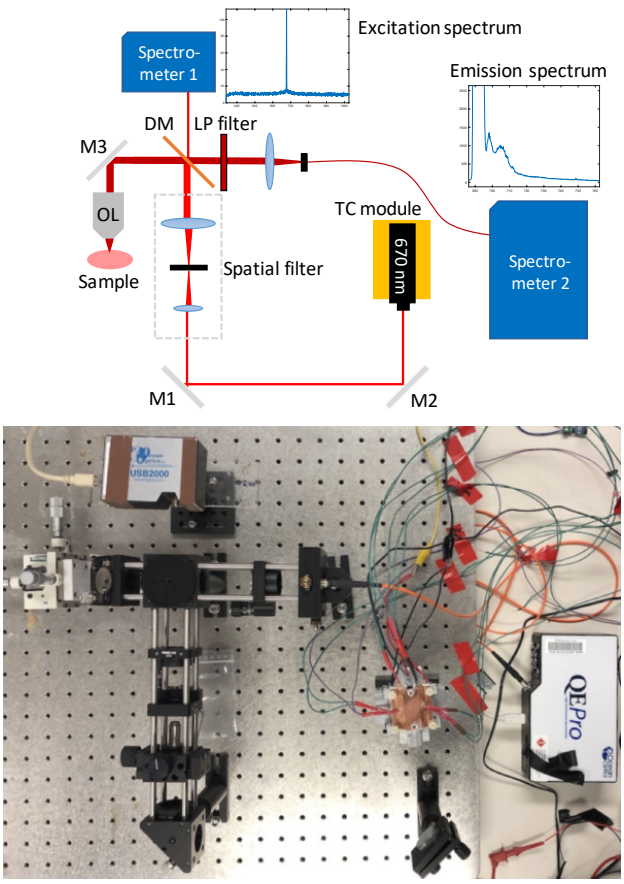

Fig. 1: Diagram and image of the confocal Raman microscope. M1,2,3: mirror 1,2,3; DM: dichroic mirror; LP filter: long pass filter; OL: objective lens; TC module: temperature control module.

Semrock), where the majority of the light was reflected and focused at the sample through an objective lens (CFI Apo NIR 40X W, 0.8NA, Nikon), while less than one per sent of the light transmitted the dichroic mirror and was collected by a spectrometer (USB2000, Ocean Optics). The focused incident light excited the sample and generated both long-shifted fluorescent and Raman emissions, which were effectively collected by the same objective lens. The collected emission light then passed the dichroic mirror and were cleaned up by a premium 685 nm long pass filter (FF01-685/LP-25, Semrock). Finally, the emission photons were coupled into a high-sensitive spectrometer (QE Pro, Ocean Optics) via a 40 mm focal-length lens (LBF254-040-B, Thorlabs) and a 25 m diameter multimode optical fiber (M68L02, Thorlabs).

The confocal Raman microscope was carefully aligned to maximize both the excitation power and signal intensity. We mounted the optical components using a cage system to simplify the alignment process. The tilt and position of the laser output beam were carefully adjusted using two kinematic mounted mirrors to make sure the beam was accurately aligned with the optical axis of the system. By fine tuning an X-Y and a Z translational mounts, we directed the laser beam through the spatial filter and got a maximum output power of 2 mW after the pinhole. Then, the cleaned-up light was collimated

by adjusting the axial position of the lens after the pinhole. In order to find the correct tilt of the dichroic mirror and mirror 3, we attached a flat mirror on the surfaces of several mounts facing perpendicularly to the optical axis of the system, and carefully adjusted each mirror's tilts until the reflected beam propagated reversely along its coming path. By doing these, we were able to obtain a maximum of 1 mW excitation power under the objective lens. In order to align the detection light path, we placed a mirror on a 3-dimensional translational stage under the objective lens. The mirror's height was fine-adjusted so that the reflected light propagated back and re-focused at the pinhole. This means the excitation light was precisely focused at the mirror's coating surface. After this process, we set the integration time of the spectrometer 2 to 1 seconds to capture the weak excitation light that reflected by the mirror and leaked through the dichroic mirror and long-pass filter. By fine-tuning two translational mounts, we could maximize the intensity of the weak leakage light, which means the emission light originated from the excitation region could also be efficiently coupled into the spectrometer.

The confocal configuration allows the microscope efficiently gathering light only from a small ellipsoid region where the sample gets irradiated and excited, thus suppressing light noises from the environments. In addition, the objective lens can focus an excitation light beam within a sub-micrometer diameter area, equipping the setup an ability to pin-point the local characters of a sample at micrometer resolutions. Moreover, compared with traditional Raman spectroscopy setups where collimated light is used for excitation, the focusing beam in confocal Raman microscope can penetrate through scattering tissues and noninvasively measure the inner Raman spectrums of a sample, which is crucial for potential healthcare applications.

B. Laser Temperature Modulation

In order to modulate and control the temperature of the laser, we used two stacked Peltier thermoelectric coolers (12V, 90W) in parallel, controlled by a Pulse Width Modulated (PWM) signal from Arduino and driven by an h-bridge from a power supply. We machined an aluminum heat sink and a copper cavity for better thermal conductivity to the laser. In order to monitor the temperatures at different points of the module, we machined several holes where thermistors were attached with thermally conductive adhesive. In the final setup, we could measure the temperature of the bottom face of the peltier (heat sink side), the temperature of the top face of the peltier (laser side), and the temperature of two points closer to the laser, which we assumed correspond to the temperature of the crystal. We can see a diagram and a picture of the Thermoelectric Cooling (TEC) module in Figure 2.

The TEC module can be used for two different purposes. On the one hand, on the one hand, we built a closed loop temperature control system to stabilize the temperature and therefore the excitation wavelength during the whole integration time to obtain a complete spectrum for a discrete temperature. With a PI controller using Arduino, the temperature of the laser could be maintained around a setpoint with an oscillation of 1°C.

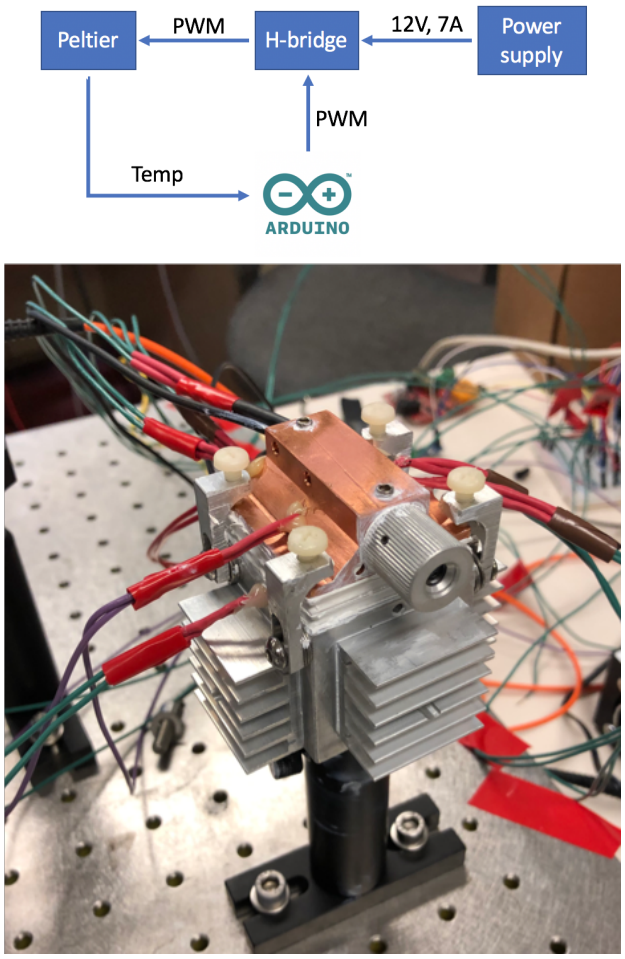

Fig. 2: Diagram and image of the peltier module. The image shows the laser inside the copper cavity, the peltier device and the aluminum heat sink with fins attached to increase heat transfer to air. Several thermistors were placed around the peltier and laser to monitor the temperature at different points.

The setpoint temperatures could range from approximately 15°C to 80°C when the ambient temperature was ∼25°C. Repeating the measurement at different fixed temperatures would allow us to reduce the fluorescent noise as explained in Section (link to section). This technique requires to measure the excitation wavelength for every set temperature and the spectrum simultaneously, and therefore we needed to use two different spectrometers, one for each measurement. On the other hand, the TEC module can also be used to stochastically vary the temperature of the laser to then characterize the relation between temperatures and laser wavelength applying system ID techniques. This approach is further explained in Section III-B.

III. Results and Discussion

A. Spectral Data Processing

The core of the spectral data processing consists of taking the difference between two shifted spectra to eliminate much

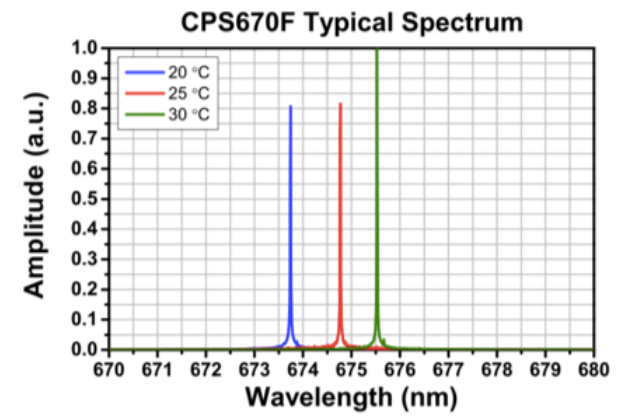

Fig. 3: Spectrum of the laser at different temperatures. It can be seen how the central wavelength of the excitation is modulated with temperature [9].

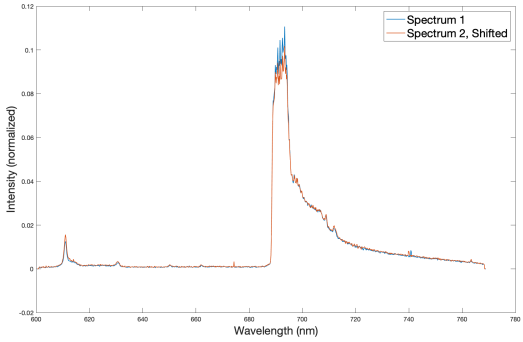

Fig. 4: Two spectrum taken of a diamond sample. Excitation wavelengths for the two spectra are: 674.7 nm for spectrum 1 and 675.3 nm for spectrum 2.

of the fluorescent background noise to increase the signal to noise ratio of the Raman signal. First, data from both spectrometers were collected and aggregated to connect the measured excitation wavelength at each time step with the spectrum. The spectra were both normalized based on the integrated intensity of the excitation wavelength to account for variation in laser power over time. The wavenumber was then calculated from the wavelength according to Equation 1.

$$\text{Raman shift } [\text{cm}^{-1}] = \frac{10^7}{\lambda_{ex}[\text{nm}]} - \frac{10^7}{\lambda[\text{nm}]} \tag{1}$$

The two spectra were subtracted and the result was then integrated to obtain the final spectrum as shown in Figure 5. This peak closely resembles published diamond Raman peaks.

B. System ID: Relating input variables to laser wavelength

In order to be able to set a desired laser wavelength sequence for eventual spectral data processing strategies, it can be very useful to characterize the TEC-laser system so as to identify what is the input signal needed to produce the targeted output. At the same time, once the system is characterized, indirectly monitoring the excitation wavelength by measuring

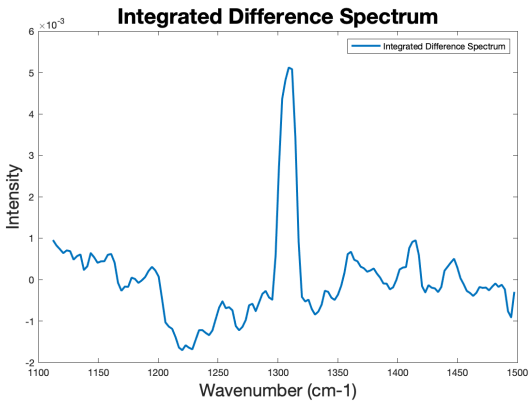

Fig. 5: Integrated difference spectrum of the diamond Raman peak showing a wavenumber of 1311 cm^{-1}

other variables in the system can help reduce the total number of components required.

1) System Diagram: The system to be characterized can be thought as a Single Input Single Output (SISO) system, where the input corresponds to the PWM signal sent from the Arduino and the output is the laser wavelength. However, before starting the system identification we know *a priori* than the system has some internal transfer functions, some of them being highly non-linear. This is shown in Figure 6.

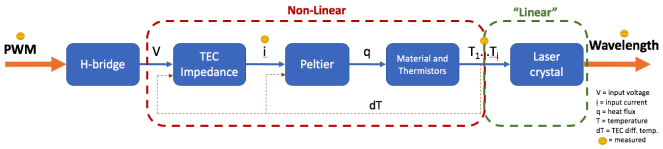

Fig. 6: System diagram showing the internal measured variables and the presence of linear and non-linear transfer functions.

2) Measured Variables: As seen in Figure 6, the variables that were monitored during the system identification process were the input PWM signal, the current sent to the TEC module, the laser wavelength, and the temperature at four different points of the setup (in the heat sink close to the TEC face ($Temp.\ TEC_{bottom}$), in the copper element close to the top TEC interface ($Temp.\ TEC_{top}$), and in two points of the copper element close to the laser diode ($Temp.\ crystal_A$ and $Temp.\ crystal_B$).

3) System non-linearities and complexity: It is known that TEC devices are intrinsically not linear and their performance is highly dependend on the difference in temperature between its hot and cold side (dT). In addition, the Joule effect makes its performance as a cooler worse than as a heating device. In other words, the heat dissipated at the hot side ($Q_h = Q_c + P_{\text{Joule}}$) is the sum of the heat absorbed at the cold side (Q_c) and the heating generated by the Joule effect ($P_{\text{Joule}} \propto I^2R$). Figure 7 shows an example of the performance of a TEC module for different input current and differential temperature 2. Therefore, we can see that dT acts as intrinsic internal feedback, which, along with the non-linearities shown in Figure 7, makes the identification of the

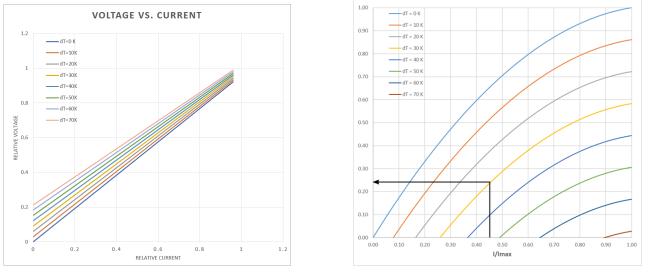

(a) TEC impedance (b) Heat absorbed on cold side

Fig. 7: Example of a TEC module performance, highlighting that it is a non-linear, multi-input system. This curves correspond to the second and fourth (only for cold side temperature) in Figure 6. Source: Meerstetter Engineering [10]

transfer function between input voltage (V) and temperatures (T) complex. Should we want to have a complete system identification we should build a multi-input system taking dT as one of the input internal variables, which is out of the scope of this paper. However, the last block in Figure 6, that is, the transfer function between the measured temperature and the wavelength should have a behaviour much closer to a SISO system, which motivated the analysis described in this section.

4) Data acquisition: To identify the dynamics of the temperature to wavelenght relationship, we generated a stochastic PWM input using our Arduino and we recorded the input current, temperatures,and laser wavelength. Since the mentionned dynamics are expected to be below 1Hz we shaped our stochastic input accordingly, where the PWM amplitude is drawn from a uniform distribution between -255 and 255 (where ± 255 are the maximum PWM levels in cooling or heating modes respectively) and each levels is held constant for N seconds, where N is uniformly sampled from [1, 30] seconds. Note that the speed of the system depends largely on the maximum current allowed by the power source. The data was taken over several thousand seconds, with a sampling rate of 5Hz. Figure 8 shows the stochastic input in one of our trials.

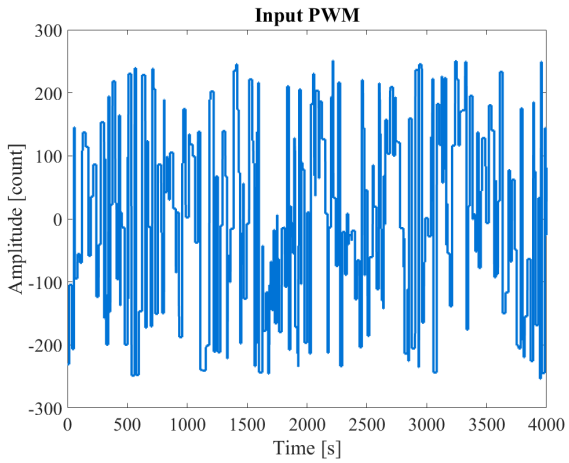

Fig. 8: PWM stochastic input in out of our experiments.

5) System ID: Applying the techniques learned in class with 20,000 samples, we estimated the impulse response of the system using the input auto-correlation (c_{XX}) and input-output cross-correlation (c_{XY}) (i.e. $h^{\mathrm{est}} := \mathrm{Toeplitz}(c_{\mathrm{XX}})^{-1}\ c_{\mathrm{XY}}$). Figure 9 is an example of the auto and cross-correlation functions found in our system. Note that in our analysis we have shifted all the data to be centered around zero. Using the estimated impulse response the output can be estimated ($y^{\mathrm{est}} = h^{\mathrm{est}} \circledast x$). Then, the quality of this estimation can be computed using two parameters: the Root Mean Squared Error (RMSE) and the Variance Accounted For (VAF), defined equations 2 and 3, respectively.

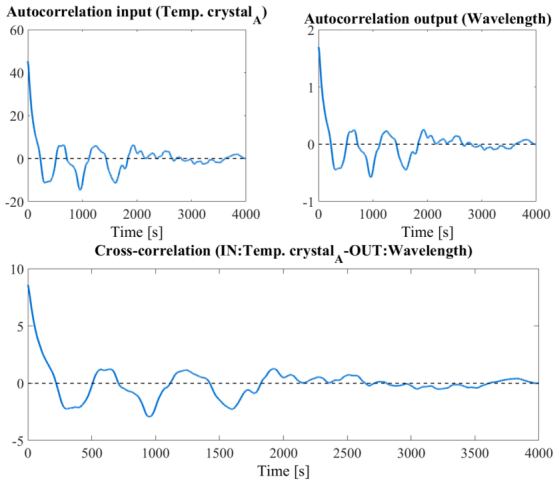

Fig. 9: Auto-correlations and cross-correlation when $Temp.crystal_A$ and the wavelength are taken as input and output of the system, respectively.

$$\mathrm{RMSE} = \sqrt{\frac{1}{N}\sum_{n=1}^{N}(y_n^{est} - y_n)^2} \tag{2}$$

$$\mathrm{VAF} = 100\left(1 - \frac{\sigma(y^{est} - y)^2}{\sigma(y)^2}\right) \tag{3}$$

We performed this analysis for all the input-output combinations and, as expected, we obtained the best results when estimating the wavelength from one of the temperature sensors close to the diode (in particular $Temp.crystal_A$). The result of this estimation is shown in Figure 10. This first analysis accounts for the 92.229% of the variance. However, to improve the estimation we added a time shift and a scale coefficient to the estimated data. These parameters where found such that they maximize the VAF and minimize the RMSE, respectively. The result is an improvement of 0.1% in the VAF and a reduction of half of the RMSE. Finally, with a VAF of 92.3% and a DMSE of .18, we can assert that the estimation of the output was successful.

IV. Conclusion

Non-invasive material characterization techniques have wide applications in a variety of fields including health care. In this paper, we built a temperature-modulated confocal Raman spectrometer to identify material samples. We tested our

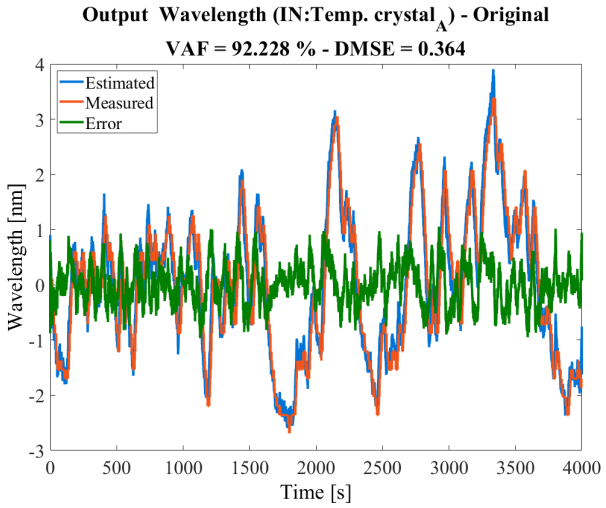

Fig. 10: Estimated and measured wavelength taking $Temp.crystal_A$ as the input.

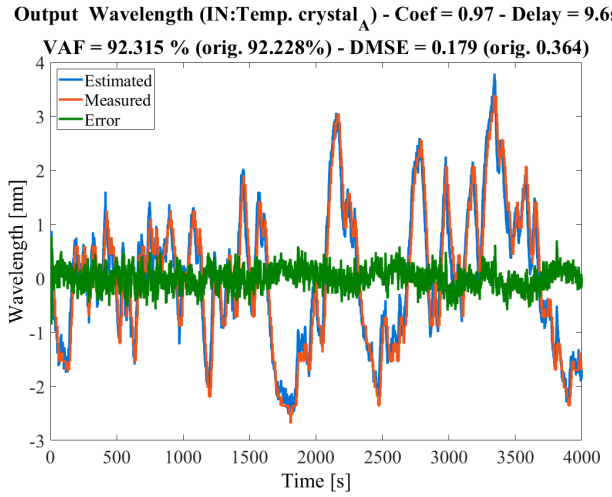

Fig. 11: Estimated wavelength adding a time shift of 9.6s and a scaling coefficient of 0.97, both found by optimization of VAF and RMSE. The improvement in the latter is significant, since it gets reduces in a 50%

system on diamond samples with artificial noise to simulate glucose underneath the skin. Our results show that by using temperature modulated laser wavelength, noise can be removed, improving the signal to noise from 2.9 to 4.3. We also performed a system identification analysis of our laser setup. Applying the techniques learned in class with 20,000 points, we computed the impulse response of the system and we estimated the output (wavelength) from the input signal. With a VAF of 92.3%, we characterized system to estimate wavelength of the laser given any temperature signal.

ACKNOWLEDGMENT

Authors would like to thank Prof.Hunter for helping us with valuable suggestions throughout the project. We would also like to thank both Span and Mike for their immense help with the project and the course nuggets.

REFERENCES

[1] Ralph Snyderman and Ziggy Yoediono. Prospective care: a personalized, preventative approach to medicine. 2006.
[2] Andrew P Shreve, Nerine J Cherepy, and Richard A Mathies. Effective rejection of fluorescence interference in raman spectroscopy using a shifted excitation difference technique. *Applied spectroscopy*, 46(4):707–711, 1992.
[3] Changan Xie and Yong-qing Li. Confocal micro-raman spectroscopy of single biological cells using optical trapping and shifted excitation difference techniques. *Journal of Applied Physics*, 93(5):2982–2986, 2003.
[4] Scott T McCain, Rebecca M Willett, and David J Brady. Multi-excitation raman spectroscopy technique for fluorescence rejection. *Optics Express*, 16(15):10975–10991, 2008.
[5] Derek Albert Long. Raman spectroscopy. *New York*, pages 1–12, 1977.
[6] PF Williams, Denis L Rousseau, and SH Dworetsky. Resonance fluorescence and resonance raman scattering: lifetimes in molecular iodine. *Physical Review Letters*, 32(5):196, 1974.
[7] JM Harris, RW Chrisman, FE Lytle, and RS Tobias. Sub-nanosecond time-resolved rejection of fluorescence from raman spectra. *Analytical Chemistry*, 48(13):1937–1943, 1976.
[8] Juha Kostamovaara, Jussi Tenhunen, Martin Kögler, Ilkka Nissinen, Jan Nissinen, and Pekka Keränen. Fluorescence suppression in raman spectroscopy using a time-gated cmos spad. *Optics express*, 21(25):31632–31645, 2013.
[9] Thorlabs Inc. CPS670F typical spectrum. Technical report, 2014.
[10] Meerstetter ENgineering. TEC peltier element design guide. Technical report, 2017.

Authors:

Zeguan Wang is a graduate student in the program of Media Arts & Sciences at MIT. His research is currently focusing on developing novel optical imaging techniques that could contribute to the understanding of the brain.

Sai Nithin Reddy Kantareddy is a graduate student in the Department of Mechanical Engineering at MIT. His research currently focuses on developing low-cost sensing methods using radio frequency backscattering techniques.

Hilary Johnson is a graduate student in the Department of Mechanical Engineering at MIT. She a researcher in the PERG group.

Álvaro Fernández Galiana is a graduate student in the Department of Mechanical Engineering at MIT. He conducts his research, focused on quantum optics and precision engineering, at the LIGO group.

Alexandre Armengol Urpi is a graduate student in the Department of Mechanical Engineering at MIT. His research currently focuses on brain signal processing.